Broadband microwave photonic fully tunable filter using a single heterogeneously integrated III-V/SOI-microdisk-based phase shifter

Juan Lloret,[1,*] Geert Morthier,[2] Francisco Ramos,[1] Salvador Sales,[1] Dries Van Thourhout,[2] Thijs Spuesens,[2] Nicolas Olivier,[3] Jean-Marc Fédéli,[3] and José Capmany,[1]

[1]*ITEAM Research Institute, Optical and Quantum Communications Group, Universitat Politècnica de València, Camino de Vera s/n, 46022 València, Spain.*
[2]*INTEC Department, Photonics Research Group, Universiteit Gent-IMEC, St. Pietersnieuwstraat 41, 9000 Gent, Belgium.*
[3]*CEA-LETI, Minatec Campus, 17 Rue des Martyrs, 38054 Grenoble, France.*
[*]*jualloso@iteam.upv.es*

Abstract: A broadband microwave photonic phase shifter based on a single III-V microdisk resonator heterogeneously integrated on and coupled to a nanophotonic silicon-on-insulator waveguide is reported. The phase shift tunability is accomplished by modifying the effective index through carrier injection. A comprehensive semi-analytical model aiming at predicting its behavior is formulated and confirmed by measurements. Quasi-linear and continuously tunable 2π phase shifts at radiofrequencies greater than 18 GHz are experimentally demonstrated. The phase shifter performance is also evaluated when used as a key element in tunable filtering schemes. Distortion-free and wideband filtering responses with a tuning range of ~100% over the free spectral range are obtained.

References and links

1. R. Soref, "The past, present and future of silicon photonics," IEEE J. Sel. Tops. Quantum Electron. **12**(6), 1678−1687 (2006).
2. W. Bogaerts, R. Baets, P. Dumon, V. Wiaux, S. Beckx, D. Taillaert, B. Luyssaert, J. Van Campenhout, P. Bienstman, and D. Van Thourhout, "Nanophotonic waveguides in silicon-on-insulator fabricated with CMOS technology," IEEE J. Lightwave Technol. **23**(1),401−412 (2005).
3. G. Roelkens, D. Van Thourhout, R. Baets, R. Notzel, and M. Smit, "Laser emission and photodetection in an InP/InGaAsP layer integrated on and coupled to a silicon-on-insulator waveguide circuit," Opt. Exp. **14**(18), 8154−8159 (2006).
4. A. W. Fang, H. Park, O. Cohen, R. Jones, M. J. Paniccia, and J. E. Bowers, "Electrically pumped hybrid AlGaInAs-silicon evanescent laser," Opt. Exp. **14**(20), 9203−9210 (2006).
5. A. W. Fang, R. Jones, H. Park, O. Cohen, O. Raday, M. J. Paniccia, and J. E. Bowers, "Integrated AlGaInAs-silicon evanescent racetrack laser and photodetector," Opt. Exp. **15**(5), 2315−2322 (2007).
6. J. Van Campenhout, P. Rojo-Romeo, P. Regreny, C. Seassal, D. Van Thourhout, S. Verstuyft, L. Di Cioccio, J.-M. Fedeli, C. Lagahe, and R. Baets, "Electrically pumped InP-based microdisk lasers integrated with a nanophotonic silicon-on-insulator waveguide circuit," Opt. Exp. **15**(11), 6744−6749 (2007).
7. J. Van Campenhout, P. Rojo-Romeo, D. Van Thourhout, C. Seassal, P. Regreny, L. Di Cioccio, J.-M. Fedeli, and R. Baets, "Design and Optimization of Electrically Injected InP-Based Microdisk Lasers Integrated on and Coupled to a SOI Waveguide Circuit," IEEE J. Lightwave Technol. **26**(1), 52−63 (2008).
8. L. Liu, T. Spuesens, G. Roelkens, D. Van Thourhout, P. Regreny, and P. Rojo-Romeo, "A Thermally Tunable III-V Compound Semiconductor Microdisk Laser Integrated on Silicon-on-Insulator Circuits," IEEE Photon. Technol. Lett. **22**(17), 1270−1272 (2010).
9. J. Van Campenhout, L. Liu, P. Rojo-Romeo, D. Van Thourhout , C. Seassal, P. Regreny, L. Di Cioccio, J.-M. Fedeli, and R. Baets, "A Compact SOI-Integrated Multiwavelength Laser Source Based on Cascaded InP Microdisks," IEEE Photon. Technol. Lett. **20**(16), 1345−1347 (2008).

10. R. Kumar, L. Liu, G. Roelkens, E.-J. Geluk, T. de Vries, F. Karouta, P. Regreny, D. Van Thourhout, R. Baets, and G. Morthier, "10-GHz All-Optical Gate Based on a III-V/SOI Microdisk," IEEE Photon. Technol. Lett. **22**(13), 981−983 (2010).

11. D. Van Thourhout, T. Spuesens, S. K. Selvaraja, L. Liu, G. Roelkens, R. Kumar, G. Morthier, P. Rojo-Romeo, F. Mandrolo, P. Regreny, Odez Raz, C. Kopp, and L. Grenouillet, "Nanophotonic Devices for Optical Interconnect," IEEE J. Sel. Tops. Quantum Electron. **16**(5), 1363−1375 (2010).

12. L. Liu, J. Van Campenhout, G. Roelkens, D. Van Thourhout, P. Rojo-Romeo, P. Regreny, C. Seassal, J.-M. Fedeli, and R. Baets, "Ultralow-power all-optical wavelength conversion in a silicon-on-insulator waveguide based on a heterogeneously integrated III-V microdisk laser" Appl. Phys. Lett. **93**, 061107 (2007).

13. R. Kumar, T. Spuesens, P. Mechet, P. Kumar, O. Raz, N. Oliver, J.-M. Fedeli, G. Roelkens, R. Baets, D. Van Thourhout, and G. Morthier, "Ultrafast and bias-free all-optical wavelength conversion using III-V-on silicon technology," Opt. Lett. **36**(13), 2450−2452 (2011).

14. L. Liu, R. Kumar, K. Huybrechts, T. Spuesens, G. Roelkens, E.-J. Geluk, T. de Vries, P. Regreny, D. Van Thourhout, R. Baets, and G. Morther, "An ultra-small, low-power, all-optical flip-flop memory on a silicon chip," Nat. Photonics **4**(3), 182−187 (2010).

15. L. Liu, J. Van Campenhout, G. Roelkens, R. A. Soref, D. Van Thourhout, P. Rojo-Romeo, P. Regreny, C. Seassal, J.-M. Fedeli, and R. Baets, "Carrier-injection-based electro-optic modulator on silicon-on-insulator with heterogeneously integrated III-V micordisk cavity," Opt. Lett. 33(21), 2518−2520 (2008).

16. A. Seeds, "Microwave photonics," Trans. Microwave Theory and Tech. **50**, 877−887 (2002).

17. J. Capmany and D. Novak, "Microwave photonics combines two worlds," Nature Photon. **1**(6), 319−330 (2007).

18. J. Capmany, B. Ortega, D. Pastor and S. Sales, "Discrete-Time Optical Processing of Microwave Signals," IEEE J. Lightwave Technol. **23**(2), 702−723 (2005).

19. J. Capmany, B. Ortega and D. Pastor, "A Tutorial on Microwave Photonic Filters," IEEE J. Lightwave Technol. **24**(1), 201−229 (2006).

20. R. W. Boyd and D. J. Gauthier, "Slow and fast light," Prog. Optics **43**, 497−530 (2002).

21. T. F. Krauss, "Why do we need slow light?," Nature Photon. **2**, 448−450 (2008).

22. M. Pu,L. Liu, W. Xue, Y. Ding, L. Hagedorn-Fradsen, H. Ou, K. Yvind and J. M. Hvam, "Tunable Microwave Phase Shifter based on Silicon-on-Insulator Microring Resonator," IEEE Photon. Technol. Lett. **22**(12), 869-871 (2010).

23. M. Pu, L. Liu, W. Xue, Y. Ding, L. Hagedorn-Fradsen, H. Ou, K. Yvind and J. M. Hvam, "Widely tunable microwave phase shifter based on silicon-on-insulator dual-microring resonator," Opt. Exp. **18**(6), 6172−6182 (2010).

24. J. Cardenas, M. A. Foster, N. Sherwood-Droz, C. B. Poitras, H. L. R. Lira, B. Zhang, A. L. Gaeta, J. B. Khurgin, P. Morton, and M. Lipson, "Wide-bandwidth continuously tunable optical delay line using silicon microring resonators," Opt. Express **18**(25), 26525−26534 (2010).

25. P.A. Morton and J. B. Khurgin, "Microwave Photonic Delay Line With Separate Tuning of the Optical Carrier," IEEE Photon. Technol. Lett. **21**(22), 869−871 (2009).

26. J. D. Doménech, P. Muñoz, and J. Capmany, "Transmission and group-delay characterization of coupled resonator optical waveguides apodized through the longitudinal offset technique," Opt. Exp. **36**(2), 136−138 (2011).

27. R. L. Espinola, M. C. Tsai, J. T. Yardley, and R. M. Osgood, "Fast and Low-Power Thermooptic Switch on Thin Silicon-on-Insulator," IEEE Photon. Technol. Lett. **15**(10), 1366−1368 (2003).

28. M. Sagues, R. García-Olcina, A. Loayssa, S. Sales and J. Capmany, "Multi-tap complex-coefficient incoherent microwave photonic filters based on optical single-sideband modulation and narrow band optical filtering," Opt. Exp. **16**(1), 295−303 (2008).

29. Y. Chen, W. Xue, F. Öhman and J. Mork, "Theory of Optical-Filtering Enhanced Slow and Fast Light Effects in Semiconductor Optical Waveguides," IEEE J. Lightwave Technol. **26**(23), 3734−3743 (2008).

30. J. Lloret, J. Sancho, M. Pu, I. Gasulla, K. Yvind, S. Sales and J. Capmany, "Tunable complex-valued multi-tap microwave photonic filter based on single silicon-on-insulator microring resonator," Opt. Exp. **19**(13), 12402−12407 (2011).

31. M. Burla, D. Marpaung, L. Zhuang, C. Roeloffzen, M. R. Khan, A. Leinse, M. Hoekman and R. Heideman, "On-chip CMOS compatible reconfigurable optical delay line with separate carrier tuning for microwave photonic signal processing," Opt. Exp. **19**(22), 21475−21484 (2011).

1. Introduction

Over the past years, silicon-on-insulator (SOI) has arisen as the preferred technology platform for implementing passive photonic functionalities. Features such as the transparency of silicon at telecom wavelengths, the high refractive index contrast, which leads to high-density integration, or the compatibility with complementary metal oxide semiconductor (CMOS)

technology offer the possibility of device fabrication in the sub-micron scale [1-2]. However, a major obstacle for large-scale silicon-based electronic-photonic integration is the indirect band gap of silicon, which results in low-efficiency light-emitting. In practice, this fact hampers the assembly of high-performance active devices.

A promising solution for implementing active functionalities using SOI platforms consists of bonding on a direct band gap material, especially those belonging to the III-V group [3-5]. In particular, InP-based approaches have become of great importance since ultra-compact cavities with low optical loss, together with sufficient confinement, have been recently demonstrated [6-7]. These properties have been exploited in InP/SOI microdisk-type resonators for the implementation of various functionalities, in the search of a multi-purpose device. Among them, tunable single-wavelength [8] and multi-wavelength [9] lasers, optical gating [10], electro-optical switching [11], wavelength conversion [12-13], all-optical flip-flop [14] and electro-optical amplitude modulators [15] have already been reported. However, to the best of our knowledge, no efforts have been accomplished using such a device within the field of microwave photonics (MWP) [16-17].

MWP enables the generation, transport and processing of radio frequency (RF), microwave and millimeter-wave signals in the optical domain [18]. In particular, reconfigurable and tunable photonic filtering of microwave signals free from bandwidth constraints has focused considerable efforts [19]. To this end, high performance tunable microwave phase shifters and true time delay lines are of key importance. For this purpose, integrated SOI slow-light-based ring resonators have found to be a very promising solution [20-21]. Specifically, quasi-linear 360° phase shifts with a power penalty of less than 2 dB have been obtained at 40 GHz in SOI dual-microring resonators [22-23]. Concerning time delaying functionalities, long tunable optical delays over wide bandwidths in novel configurations based on cascaded SOI microrings have also been demonstrated [24, 26]. Besides, the separate carrier tuning technique has been recently used for overcoming the inherent bandwidth limitation when employing microrings [25]. However, the main drawback of SOI-based approaches is connected to its tunability speed. Tunability is commonly carried out by modifying the group index through thermo-optic effects. Therefore, the tunability speed is limited by the silicon thermal dynamics, resulting in tuning times in the scale of hundreds of microseconds [27].

In this paper, a novel MWP fully-tunable phase shifter comprised of a single InP-based microdisk resonator (MDR) integrated on and coupled to a nanophotonic SOI waveguide fabricated through bonding technology is presented and demonstrated. The tuning control mechanism is based on carrier injection, rather than on the adjustment of the optical wavelength [22] or thermo-optic effects [23]. In this way, the tuning speed limitation is circumvented as dynamics as fast as hundreds of picoseconds can be reached in InP-based materials, resulting in an improvement by more of six orders of magnitude. Finally, the phase shifter is used as a key element in a notch-type filtering scheme yielding distortion-free and wideband response with a tuning range ~100% over the free spectral range (FSR).

2. Principle of operation

A schematic drawing of the device structure is sketched in Fig. 1(a). It basically consists of an InP-based MDR cavity with radius R, which is bonded onto a Si waveguide featuring a power coupling factor k. $E_{in}(t,z)$ and $E_{out}(t,z)$ correspond to the input and output electrical fields respectively. Fig. 1(b) shows the principle of operation of the InP/SOI MDR based MWP phase shifter. The propagation in such a structure is based on whispering-gallery modes (WGMs), which are confined to the edges of the MDR resulting in a resonant-type response. If an optical single-sideband (OSSB) modulation signal is inserted at the input and accurately placed in the vicinity of a resonance, the optical carrier and the modulation sideband will experience different phase changes according to their spectral positions in the MDR phase transfer function. By acting on the carrier injection into the MDR, the effective index can be

modified and consequently the spectral positions of the resonances can be shifted. In this way, the difference between the optical phase shifts experienced by the optical carrier and the sideband can be changed. Both the input optical power and the injection current can be used as control mechanisms for the carrier density (N) thus allowing for controllable tuning of the phase shift difference. Upon beating at the optical detector, this phase shift difference is impressed onto the resulting microwave carrier.
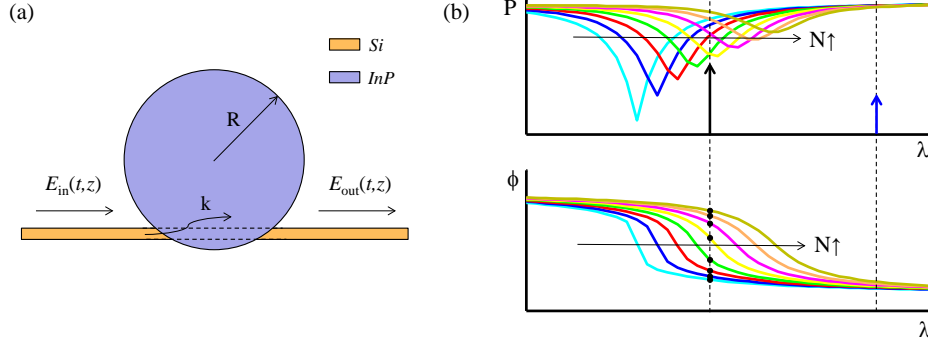

Fig. 1. (a) Schematic drawing of the heterogeneous InP MDR showing the SOI wire waveguide. (b) Principle of operation of the MDR-based MWP phase shifter when using OSSB at its input.

The technique of combining OSSB modulation with optical filtering to implement complex-valued filters was originally proposed in [28], where phase shifters based on fiber Bragg gratings (FBG) instead of InP/SOI MDRs were considered.

Hereafter, a comprehensive semi-analytical analysis aiming at predicting the device behavior is derived. To avoid loss of generality, a double-sideband signal comprised of an optical carrier at optical frequency ω_0 and two sidebands at $\omega_0 \pm \Omega$ is considered at the MDR input

$$E_{in}(t,z) = \left(|E_0(z)| e^{j\theta_0} + |E_{-1}(z)| e^{j(\Omega t + \theta_{-1})} + |E_{+1}(z)| e^{-j(\Omega t - \theta_{+1})} \right) e^{-j(\omega_0 t - k_0 z)}, \qquad (1)$$

where k_0 is the propagation constant and Ω is the modulation frequency. $|E_0|$ and θ_0 correspond to the amplitude modulus and optical phase of the optical carrier, whereas $|E_{+1}|$, $|E_{-1}|$, θ_{+1} and θ_{-1} are those corresponding to the blue and red shifted modulation sidebands, respectively. Equation (1) can be particularized for OSSB modulation by assuming $|E_{+1}|=0$ or $|E_{-1}|=0$. Harmonic distortion effects are neglected because small-signal modulation is considered.

After the transient time, the optical complex field at the MDR output can be expressed as a function of the transmission coefficient, T, as

$$E_{out} = \left(\frac{T - |H| e^{j\phi}}{1 - T|H| e^{j\phi}} \right) E_{in}, \quad \text{with} \quad T = \sqrt{1 - k^2}, \qquad (2)$$

being $|H|$ and ϕ the amplitude modulus and the phase of the resonant cavity's transfer function, respectively. $T|H| < 1$ has to be fulfilled to reach the steady state. Therefore, the device must be operated below threshold.

The derivation of the cavity transfer function involves the assessment of the propagation equations for all the three optical waves. The propagation equations are formulated in the context of a wave mixing description. Wave mixing in active semiconductor materials has contributions from carrier density depletion, carrier heating, spectral hole burning, two-photon absorption and Kerr effects. However, for modulation frequencies up to some tens of GHz, the dominating mechanism mediating the wave mixing is the carrier density pulsation [29]. In this manner, the ultrafast effects as well as the gain saturation due to amplified emission noise are

neglected, which are reasonable approximations in the regime of moderate input optical power. Consequently, the wave mixing problem can be simplified by accounting just for the interactions between the three optical waves as

$$\frac{\partial E_0}{\partial z} = \gamma_0 E_0,$$

$$\frac{\partial E_{-1}}{\partial z} = \gamma_0 E_{-1} + \varepsilon_{-1}\left\{|E_0|^2 E_{-1} + E_0^2 E_{+1}^* e^{j\Delta kz}\right\},$$

$$\frac{\partial E_{+1}}{\partial z} = \gamma_0 E_{+1} + \varepsilon_{+1}\left\{|E_0|^2 E_{+1} + E_0^2 E_{-1}^* e^{j\Delta kz}\right\}, \tag{3}$$

where γ_0 and $\varepsilon_{\pm1}$ are the complex first- and third-order susceptibilities, respectively. Δk is the phase-mismatching factor induced by the background and the waveguide dispersions. $\Delta k = 0$ is a good approximation when considering modulating frequencies up to several tens of GHz. Besides, E_0, E_{-1} and E_{+1} refer in this case to the optical waves already travelling inside the cavity.

By solving the set of differential equations depicted in (3) analogously to [29], the electrical field for all the three optical waves can be expressed as

$$E_0(z = L) = E_0(z = 0)e^{F(L)},$$

$$E_{-1}^*(z = L) = e^{F(L)^*}\left\{\frac{1}{2}\left(-v(0) + u(0)\left[j\alpha\left(e^{G(L)} - 1\right) + e^{G(L)}\right]\right)\right\},$$

$$E_{+1}(z = L) = e^{F(L)}\left\{\frac{1}{2}\left(v(0) + u(0)\left[j\alpha\left(1 - e^{G(L)}\right) + e^{G(L)}\right]\right)\right\}, \tag{4}$$

with

$$u(0) = E_{+1}(z = 0)e^{-F(L)} + E_{-1}^*(z = 0)e^{-F(L)^*},$$

$$v(0) = E_{+1}(z = 0)e^{-F(L)} - E_{-1}^*(z = 0)e^{-F(L)^*}. \tag{5}$$

Where $F(L)$ and $G(L)$ respectively stand for the common and the gain grating related complex amplification factors for the device length $L=2\pi R$ [29].

By referring (4) to the electrical field at the input, the MDR transfer function $H=|H|e^{j\phi}$ can be derived for all the three optical waves as

$$H_0 = e^{F(L)},$$

$$H_{-1}^* = \frac{1}{2}\left\{\begin{array}{l}1 + \frac{E_{+1}(z=0)}{E_{-1}^*(z=0)}e^{-F(L)}e^{F(L)^*}\left[j\alpha\left(e^{G(L)} - 1\right) + e^{G(L)} - 1\right] + \\ j\alpha\left(e^{G(L)} - 1\right) + e^{G(L)}\end{array}\right\},$$

$$H_{+1} = \frac{1}{2}\left\{\begin{array}{l}1 + \frac{E_{-1}^*(z=0)}{E_{+1}(z=0)}e^{F(L)}e^{-F(L)^*}\left[j\alpha\left(1 - e^{G(L)}\right) + e^{G(L)} - 1\right] + \\ j\alpha\left(1 - e^{G(L)}\right) + e^{G(L)}\end{array}\right\}. \tag{6}$$

Equations (6) have to be inserted into equation (2) to obtain the output complex electrical field for each optical wave. After photodetection, the current beating term oscillating at Ω is then

$$i_\Omega(t) \propto 2\Re\left\{|E_{out,0}||E_{out,-1}|\cos\left(\Omega t + \left(\theta_{out,0} - \theta_{out,-1}\right)\right) + |E_{out,0}||E_{out,+1}|\cos\left(\Omega t + \left(\theta_{out,+1} - \theta_{out,0}\right)\right)\right\}, \tag{7}$$

where t refers to time, $\Re$ is the detector responsivity and $\theta_{out,i}=\arg(E_{out,i})$, for i = −1,0 or 1.

Finally, the electrical power and the phase shift of the microwave output signal is calculated as

$$P_\Omega = \left| i_\Omega \right|^2 Z_0,$$
$$\Delta\varphi = \arg\left\{ i_\Omega \right\} - \arg\left\{ i_\Omega \right\}\big|_{ref}, \tag{8}$$

where Z_0 is the input impedance of the detector. The phase shift is stated relative to a reference, which is defined attending to the minimum carrier density. In this particular case, $|E_{+1}|=0$ because OSSB is inserted into the MDR.

3. Phase shifter implementation

Fig. 2(a) sketches the experimental setup of the InP/SOI MDR based MWP phase shifter. A CW tunable laser generates a weak spectral line centered at 1562 nm. The input RF signal, $s_{in}(t)$, is imprinted onto the optical carrier by means of an intensity modulator (IM) operated in dual-drive configuration, giving as a result OSSB modulation. The signal at the output of the modulator, which is comprised of two optical waves, is sent into the MDR. Both optical waves are then weighted and phase-shifted accordingly to the MDR transfer function, which can be spectrally shifted by modifying the effective index. To this end, a tunable voltage source is connected to the metal contacts of the MDR with the aim of controlling the carrier injection. Polarization controllers are inserted at both the modulator and the MDR input to avoid power penalty derived from polarization mismatching. Finally, the optical signal exiting the MDR output is detected using a high-bandwidth photodetector (HBW PD), amplified by means of a high-gain electrical amplifier (EA) and acquired by a vectorial network analyzer (VNA) in order to measure the system transfer function.
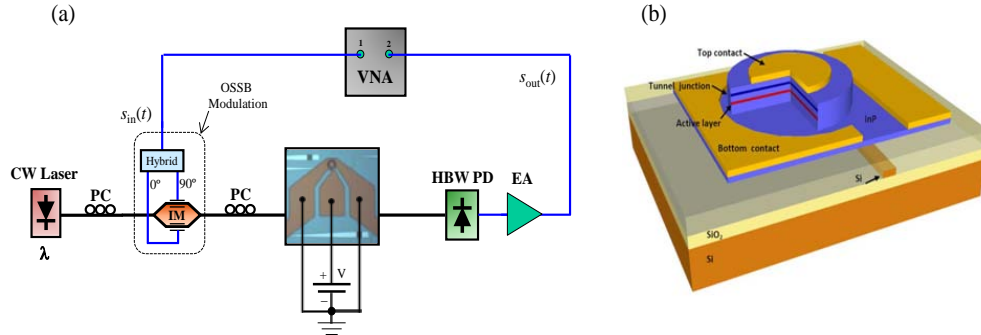

Fig. 2. (a) Experimental setup for the MWP phase shifter. (b) Schematic drawing of the heterogeneous MDR structure.

Fig. 2(b) shows the schematic drawing of the heterogeneous MDR structure, showing the InP cavity, the SOI waveguide, the bottom and top metal contacts, the tunnel junction and the active layer. The 9-µm-diameter MDR, which includes a tunnel junction for loss minimization purposes, is integrated on top of a SOI waveguide circuit containing a 750-nm-wide and 220-nm-high Si strip waveguide using molecular bonding. Under bias-free conditions the effective index is 3.474, which corresponds to a FSR of 3.054 THz (see Fig. 3(a)). The width and depth of the periodic response notches are partly fixed by the coupling disk-to-waveguide gap, featuring in this case a k of ~ 6 %. The total area, including both the input and output vertical grating couplers is around 0.1 mm². More thorough details on the fabrication of such a device are given in [11].

The gain transfer function of the device as a function of the injected current is illustrated in Fig. 3(a). The gain parabolic profile is as a consequence of the input and output vertical grating couplers efficiency with the wavelength. The notch-type transfer function can be progressively tuned by applying different currents. It is important to notice that the notch depth depends on the current as well. By increasing the current, the roundtrip loss in the cavity decreases due to a higher gain in the III-V layer. Conversely, for lower currents the roundtrip losses are greater than the k resulting in sub-coupled regime. Critical coupling gives

the maximum notch depth, which occurs for an injection current somewhere close to 0.75 mA, in which both the loss and the *k* are identical. Over-coupled regime, which means a lower loss value than *k*, is obtained when applying currents from 0.75 mA on approximately. To develop phase-shifting functionalities, the over-coupled operating regime is desired because a lower power penalty compared to the critical case is featured and still 2π phase transitions in each notch are obtained (see Fig. 3(b)). This fact sets the minimum injection current to be applied. On the other hand, the upper current limit is imposed by the threshold level. In the inset of Fig. 3(a), the relative change in the resonance placement as a function of the injected current is plotted. This spectral shift is as a result of the effective index modification due to the generation of free carriers, in combination with the thermo-optic effect. The tuning rate is fitted to be 0.8 nm/mA when considering over-coupling.

The resonance placed around 1561.5 nm was chosen for two reasons: the first because minimum insertion losses are achieved, the second because it is placed inside the telecom wavelength region. Fig. 3(b) shows a zoomed image of the mentioned resonance. Both the gain and phase transfer functions with the injection current are depicted. Not only can the different operating regimes be distinguished attending to the gain, but also to the phase-shift feature. Large phase change is only achieved when the structure is under critical or over-coupled regime.
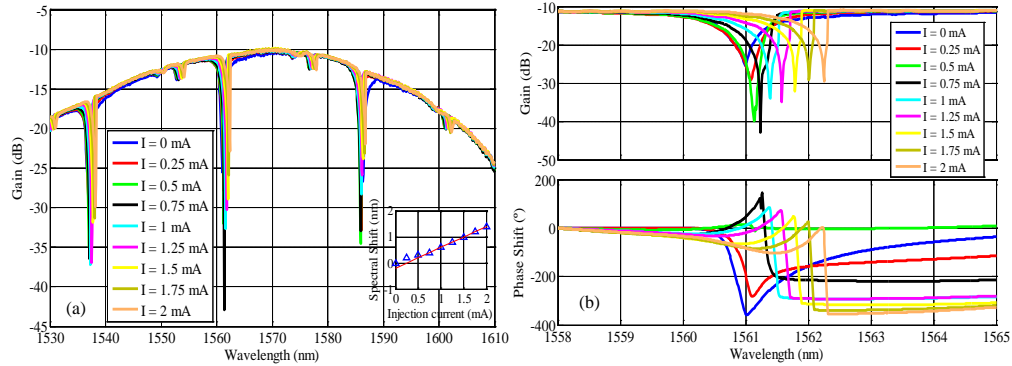

Fig. 3. (a) Measured transfer function with the injection current. In the inset, the spectral shift of the resonance when changing the injection current. (b) Zoomed image of the measured gain and phase transfer functions.

Table 1. Main parameters used for numerical calculations.

Symbol	Definition	Value
R	MDR radius	4.5 µm
k	Power coupling factor	6 %
Z_0	Detector input impedance	50 Ω
τ_s	Carrier lifetime	90 ps
a	Differential gain	$0.5 \cdot 10^{-20}$ m^2
α	Linewidth enhancement factor	6
a_{int}	Internal losses	4400 m^{-1}
N_t	Carrier density at transparency	$0.8 \cdot 10^{-24}$ m^{-3}
Γ	Confinement factor	0.4
P_{sat}	Saturation power	3 dBm

Detailed gain and phase transfer functions for a current range between 1.5 and 1.8 mA are illustrated in Fig. 4(a). Both experimental (solid lines) and numerical (dashed lines) results, derived from the model presented in a previous section, show a good agreement. The values of the main parameters used for the numerical calculations are given in Table 1. The total

optical power inserted at the input vertical grating coupler is 1 dBm. Misalignments are mostly due to the nonsymmetrical behavior of the resonances. In the inset of Fig. 4(a), the spectral placement for both the optical carrier and the modulation sideband within the phase transfer function are also depicted. The optical carrier is fixed and centered at 1562 nm, whereas the frequency of the modulating signal is adjusted from 5 to 20 GHz. When sweeping the injection current from 1.5 to 1.725 mA approximately, the carrier experiences a phase change of nearly 360º. Figure 4(b) shows the experimental (solid lines) and numerical (dashed lines) results for both the phase shift and the power of the detected microwave signal as a function of the injection current. It can be seen that quasi-linear and continuously tunable phase shifts are obtained. The maximum achievable phase shift at a certain frequency is limited by the abruptness of the phase slopes of the transfer function. In particular, a minimum modulating frequency of 18 GHz is required to reach a phase shift of $\sim 2\pi$ in this case. The functionality as a phase shifter is also demonstrated for lower frequencies, however, full 360º shifts are not obtained. In such cases, the use of cascaded MDRs represents a suitable solution to enhance the total phase shift. Specifically, by cascading m identical MDRs, the maximum phase shift can be extended by a factor of m. According to the gain transfer function, a phase change is accompanied by a power penalty. A power variation of ~ 12 dB within the tunability range comprising from 1.5 to 1.725 mA is obtained when $\Omega = 18$ GHz.
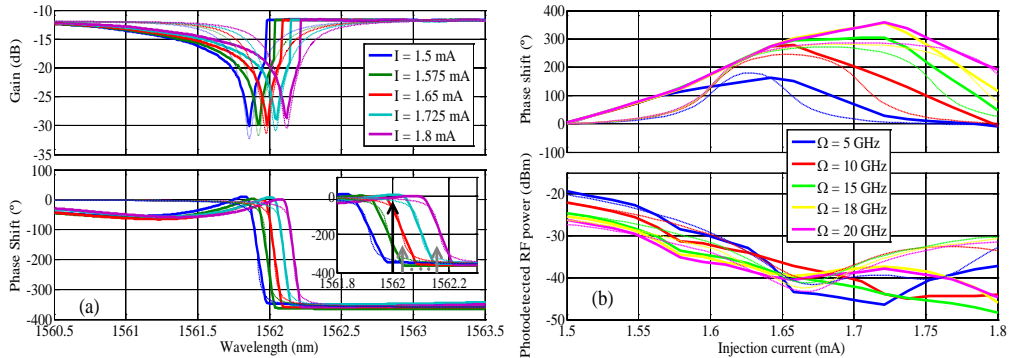

Fig. 4. (a) Detail of the measured (solid lines) and calculated (dashed lines) transfer functions considering injection currents from 1.5 to 1.8 mA. (b) Measured (solid lines) and calculated (dashed lines) phase shifts and photodetected powers of the microwave signal as a function of the injection current for different frequencies.

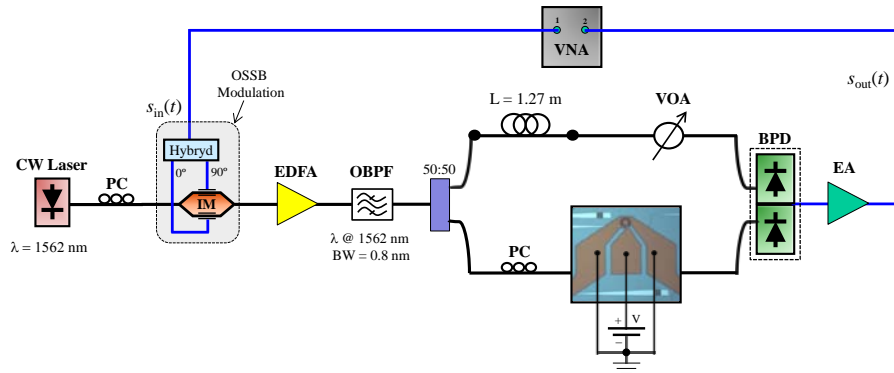## 4. Filter implementation

Fig. 5. Experimental setup of the complex-valued two-tap MWP tunable filter.

The suitability of using III-V/SOI-based MDR for implementing MWP phase shifters has been demonstrated in previous sections. Next, this feature is exploited by implementing MWP tunable filtering schemes with complex-valued coefficients. Complex-valued samples in finite impulse response (FIR) filter schemes enables controllable basic phase shift. The capability of

changing the basic phase shift results in response tunability without altering the FSR. Hereafter, a proof-of-concept approach involving two taps has been assembled. However, the design can be extended to any arbitrary number of samples.

The experimental setup for the MDR-based MWP filter is sketched in Fig. 5. The MDR is inserted in the lower arm of the interferometric structure. In this manner, the basic phase shift between both taps can be controlled by properly adjusting the injection current into the MDR. The interferometric structure is characterized by a length imbalance of 1.27 m, which corresponds to a notch-type response with a FSR of roughly 163 MHz. A variable optical attenuator (VOA) is used in the upper arm to enhance the rejection level. At the output of the IM, the OSSB signal is amplified by means of an erbium doped fiber amplifier (EDFA). An optical 0.8-nm-wide bandpass filter (OBPF) centered at the carrier wavelength is also used for noise suppression purposes. To avoid coherent-related problems, a balanced photodetector (BPD) is used.

In order to obtain the maximum tunability range, the center frequency of the filter must be high enough to be phase-shifted up to 360º. Moreover, zero phase imbalance between the minimum and maximum frequency along the filter bandwidth is required to guarantee distortion-free filter transfer function. Attending to these requirements, a center frequency of 20 GHz and an operating bandwidth of 1 GHz have been chosen, i.e. from 19.5 GHz to 20.5 GHz. Therefore, the maximum operating bandwidth attending to a specific center frequency is completely set by the phase slope abruptness of the MDR phase transfer function. Figure 6 displays the normalized filter frequency response for different injection currents into the MDR. Experimental (symbols) and theoretical (solid lines) results show a good agreement. The small deviations are attributed to reflections in the electrical part of the setup, the residual unwanted sideband in the OSSB modulation and the spontaneous noise. Nearly 2π controllable basic phase shift ($\Delta\phi$) over the operating bandwidth leads to continuously ~100% fractional tuning of the filter response.
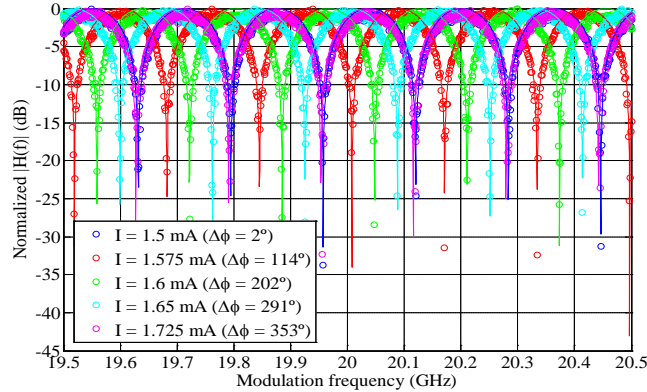

Fig. 6. Normalized frequency response of the MWP tunable filter for different injection currents.

The exploitation of the phase feature provided by ring-type resonators when implementing tunable MWP filters has been previously demonstrated using different schemes based on Si [30-31]. However, this approach offers unique properties in the context of tuning speed, which is governed by the fast dynamics in the semiconductor.

5. Summary and conclusions

A novel ultra-small and low-power broadband MWP phase shifter based on a single III-V/SOI MDR in combination with OSSB modulation has been proposed and demonstrated. Quasi-linear and continuously tunable ~360º phase shifts have been experimentally obtained when considering radiofrequencies greater than 18 GHz. Phase shift tunability is accomplished by modifying the effective index through carrier injection in the III-V layer. As a consequence,

the tunability speed is limited by the carrier dynamics in the semiconductor, which is in the scale of hundreds of ps. This fact greatly improves the performance compared to other similar Si-based approaches, in which the thermo-optic effect is used as tunable mechanism. A semi-analytical model has been derived, whose results are in good agreement with the measurements. Finally, the phase shifter is exploited for implementing complex-valued coefficients in tunable MWP filtering schemes. A proof-of-concept implementation involving two taps is demonstrated. Distortion-free and high-bandwidth filter responses with tuning range of ~100% over the FSR have been obtained.